JACS
JOURNAL OF THE AMERICAN CHEMICAL SOCIETY
pubs.acs.org/JACS
Article

Unimolecular Chiral Stepping Inversion Machine

Yonghui Sun, Lijuan Liu, Linnan Jiang, Yong Chen, Hengyue Zhang, Xiufang Xu, and Yu Liu*

Cite This: J. Am. Chem. Soc. 2023, 145, 16711−16717
Read Online
ACCESS | Metrics & More | Article Recommendations | Supporting Information

ABSTRACT: Intelligent molecular machines that are driven by light, electricity, and temperature have attracted considerable interest in the fields of chemistry, materials, and biology. Herein, a unimolecular chiral stepping inversion molecular machine (SIMM) was constructed by a coupling reaction between dibromo pillar[5]arene and a tetrathiafulvalene (TTF) derivative (PT3 and PT5). Compared with the longer aliphatic linker PT5, PT3 with a shorter aliphatic linker shows chiral stepping inversion, achieving chiral inversion under a two-electron redox potential. Benefiting from the successive reversible two-electron redox potential of TTF, the self-exclusion and self-inclusion conformational transformations of SIMM can proceed in two steps under redox, leading to the chirality step inversion in the pillar[5]arene core. Electrochemical experiments and circular dichroism (CD) spectra show that the redox processes can cause SIMM CD signaling to reversibly switch. More importantly, as the oxidant $Fe(ClO_4)_3$ was increased from 0.1 to 1 equiv, the CD spectral signal of SIMM disappeared at 1 equiv, and further addition of $Fe(ClO_4)_3$ resulted in the CD signal reversed from positive to negative at 309 nm, indicating that the chirality was reversed after chemical oxidation and reached a negative maximum with the addition of 2 equiv $Fe(ClO_4)_3$; thus, redox-triggered chiral stepping inversion was achieved. Furthermore, the chiral inversion can be restored to its original state after the addition of 2 equiv of reducing agent, sodium ascorbate. This work demonstrates unimolecular chiral stepping inversion, providing a new perspective on stimulus-responsive chirality in molecular machines.

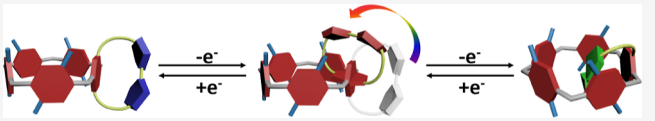

INTRODUCTION

Molecular mechanical motions that occur in response to external stimuli are fascinating, and an in-depth understanding and precise strategy to regulate these processes offer an efficient way to imitate nature, as well as provide direction for producing new materials.[1−4] Among them, unimolecular chiral regulation under a stimulus response is of great significance. Through the ingenious design and organic synthesis of stimuli-responsive molecules, they have been successfully applied to chemical sensing,[5−8] enantioselective catalysis,[9,10] nanoscience,[11−14] and enantioseparations.[15,16] In the construction of molecular machines, macrocyclic compounds, such as cyclodextrins and calixarenes, are important components that play a key role in rotaxanes, light switching, and artificial channels.[17−19] In particular, macrocyclic pillar[5]arene, which can not only construct chiral gemini-catenanes but can also be used in chiral switches, have attracted considerable attention in recent years.[20−24] The difference in the substitution position of the alkoxy groups makes the pillar[5]arenes have planar chirality; the aromatic units can be rapidly rotated around the methylene bridge and thus difficult to resolve.[25−27] By integrating the side ring on a pillar[5]arene unit, the rotation of the aromatic unit can be inhibited, thus generating a pair of separable and stable enantiomers (pS and pR); each enantiomer will undergo conformational transformation under certain stimulation, thus changing the chirality. In recent years, research on multistimuli-responsive chiral inversion based on pillar[*n*]arenes has developed rapidly. For instance, Ogoshi and co-workers reported a planar chiral pseudo[1]catenane based on pillar[5]arene, which shows complete chiral inversion after capture or release of achiral guests and solvents.[28] Yang and co-workers exhibited the temperature-driven chiral inversion of a bicyclic pillar[5]arene-based molecular universal joint, which depends on the properties of solvent and the fused ring in the pillar[5]arene.[29] Huang and co-workers reported an acid/base responsive unimolecular chirality switch based on a pillar[5]azacrown *pseudo*[1]catenane (PN4), and by adjusting the gain and loss of protons in PN4 unit, its conformation can be converted, resulting in chiral inversion.[30] Lee and co-workers reported an example of chiral inversion driven by metal ion under the control of anions based on pillar[5]thiacrown.[31] Recently, Yang and co-workers demonstrated a bicyclic pillar[6]arene derivatives molecular chiroptical switch based on azobenzene fusion, in which the photoisomerization of azobenzene can regulate its self-inclusion and self-exclusion in the pillar[6]-arene cavity, achieving optically controlled chiral inversion.[32] Although some research has been carried out in this field, chiral stepping inversion with a successive reversible two-electron redox potential has not been reported to the best of our knowledge.

Received: April 28, 2023
Published: July 24, 2023

https://doi.org/10.1021/jacs.3c04430
J. Am. Chem. Soc. 2023, 145, 16711−16717

Scheme 1. (a) Chemical Structures of PT3, PT5, and A. (b) Representation of the In−Out/Rp−Sp Equilibrium of a Pair of Enantiomers

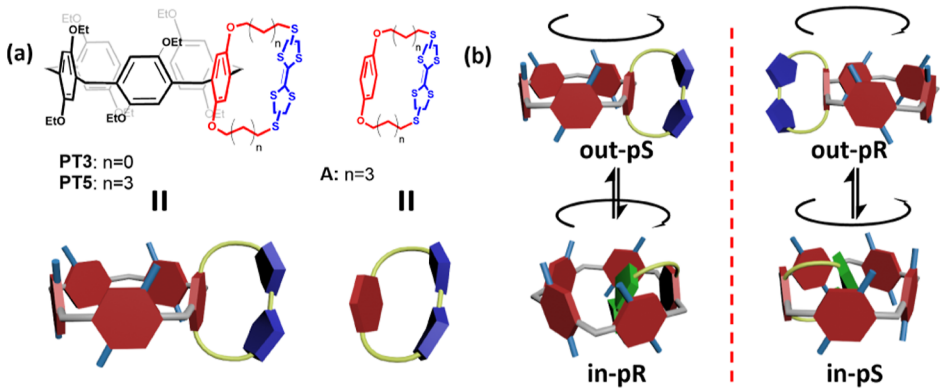

On the other hand, the revolutionary discovery of "organic metals" based on tetrathiafulvalene (TTF) boosted the development of TTF derivatives in the applications of organic conducting materials,[33−35] supramolecular chemistry,[36−38] and molecular machines.[39−41] This importance is partially based on the observation that the derivatives can act as "functional materials" and respond to various environmental inputs.[42,43] In the present study, we constructed a new chiral stepping inversion machine by integrating the redox-active TTF into one pillar[5]arene, in which TTF is a good electron donor with two reversible and easily accessible oxidation processes to its radical cation ($TTF^{\bullet+}$ radical dot) and dication (TTF^{2+}) states (Scheme 1a).[44] PT3/PT5 has two enantiomers (pS and pR). Because each enantiomer has a conformational balance between outside and inside, two pairs of atropisomers (out-pS and in-pR and out-pR and in-pS) are generated. Benefiting from the electron-donating properties of TTF, they can achieve conformational transformation under redox (Scheme 1b); in the reduced form, TTF units tend to stay outside the cavity of pillar[5]arene; when $Fe(ClO_4)_3$ is added, the TTF loses electrons and forms $TTF^{\bullet+}/TTF^{2+}$. Since the size of TTF is smaller than that of the cavity size of the pillar[5]arene, the TTF ring inverts inward, resulting in corresponding chiral changes, and conformational and chiral properties are recovered upon the addition of reducing agents. To our surprise, PT3 with a shorter aliphatic linker achieved chirality stepping inversion under two-electron redox, while PT5 with a longer aliphatic linker achieved one-electron redox chirality inversion because of the more flexible longer aliphatic linker making the one-electron TTF units more likely to occupy the cavity of PT5.

RESULTS AND DISCUSSION

The interaction between reduced TTF and pillar[5]arene was studied by a 1H NMR titration experiment. As shown in Figures S21 and S22, after adding 12.0 equiv pillar[5]arene, H_B' on TTF shows weak downfield shifts ($\Delta\delta$ = 0.05 ppm), which indicates a fast chemical exchange process. The binding constant between pillar[5]arene and TTF was determined to be (8.6 ± 2.6) M^{-1}, and the stoichiometric ratio was determined to be 1:1 (Figure S23 and Supporting Information). Due to the electron-rich cavity of pillar[5]arene, pillar[5]arene may form a more stable complex with cationic TTF^{2+}.[45,46] Consequently, TTF^{2+} was expected to be a suitable guest to more strongly bind pillar[5]arene, although TTF exhibited an extremely weak binding affinity. Since Fe^{3+} is paramagnetic, we chose diamagnetic Hg^{2+} as the oxidant and used NMR techniques to investigate its host−guest complexation after oxidizing TTF with excess Hg^{2+}. As shown in Figure 1, the disappearance of the signal at 6.1 ppm indicates

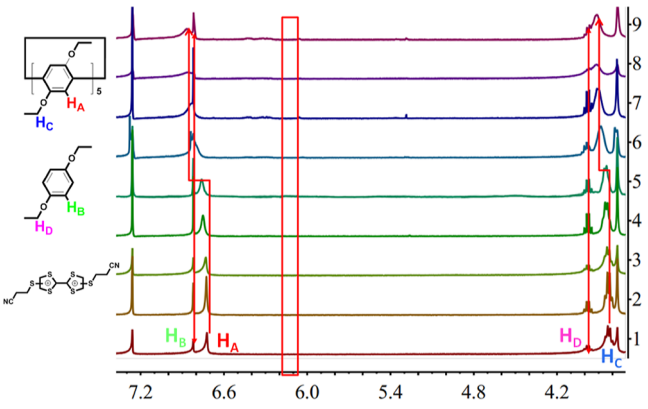

Figure 1. Partial ^{1}H NMR spectra (400 MHz, 298 K, $CDCl_3$) of pillar[5]arene (2.0 mM) in the presence of increasing concentrations of TTF^{2+} (mM): (1) 0.00, (2) 0.20, (3) 0.4, (4) 0.6, (5) 0.8, (6) 1.0, (7) 2.0, (8) 4.0, and (9) 6.0. H_A and H_C are generated from free hosts. H_B and H_D are generated from *p*-diethoxybenzene.

sufficient oxidation. The H_C and H_D protons on the reference molecule *p*-diethoxybenzene underwent little chemical shift with the addition of TTF^{2+}, whereas the H_A and H_B protons of the phenyl protons on the pillar[5]arene resulted in significant chemical shifts upfield, suggesting that the electron-deficient TTF^{2+} enters the electron-rich cavity of the pillar[5]arene. These results strongly suggest the formation of the highly stable 1:1 pillar[5]arene and TTF^{2+} inclusion complexes. The binding constant was further determined to be (2.51 ± 0.72) × 10^3 M^{-1}. In addition, two-dimensional nuclear Overhauser effect spectroscopy (NOESY) NMR spectra showed significant NOE signals between the protons H_a/H_b of TTF^{2+} and the protons H_c and H_d of methylene, indicating the inclusion of TTF^{2+} in the cavity of pillar[5]arene (Figures S24 and S25, Supporting Information).

Tetrathiafulvalene-fused bicyclic pillar[5]arene derivatives PT3 and PT5 were synthesized by a coupling reaction in a 16.5% yield, and the target molecules were fully characterized by NMR and HR-MS (Scheme S1 and Figures S1−S20, Supporting Information).

https://doi.org/10.1021/jacs.3c04430
J. Am. Chem. Soc. 2023, 145, 16711−16717

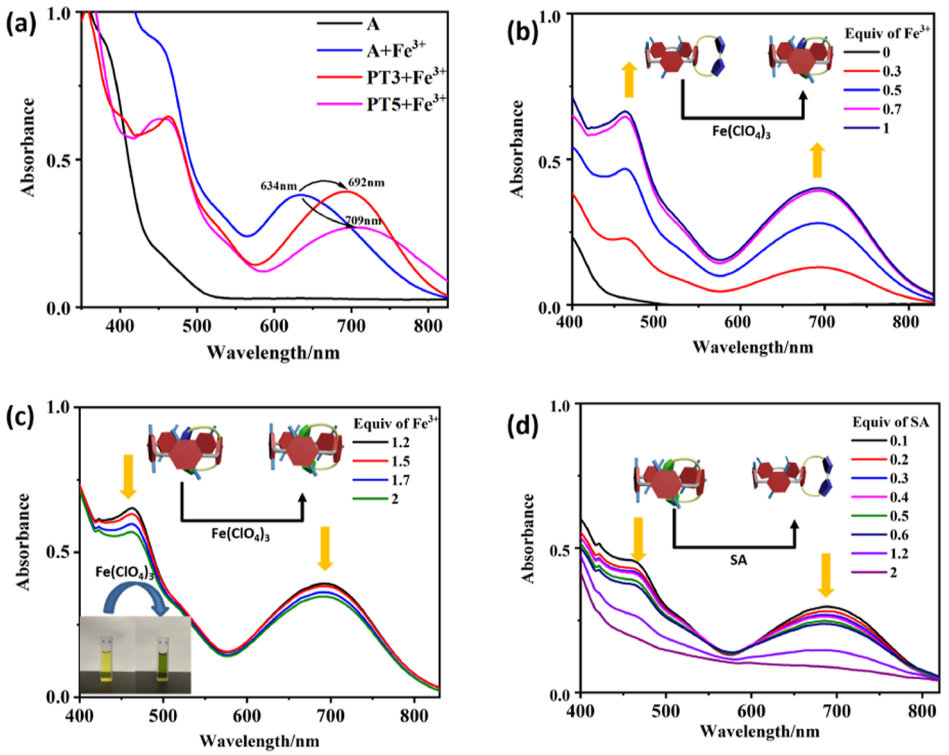

Figure 2. (a) UV−vis spectra of A, PT3, and PT5 (1×10^{-5} M in CH_3Cl) before and after the addition of 1 equiv $Fe(ClO_4)_3$. (b,c) UV−vis spectra of PT3 (1×10^{-5} M) in CH_3Cl in the presence of different amounts of $Fe(ClO_4)_3$. Inset: the solution color change in PT3 before (light yellow) and after (light green) the addition of 1 equiv $Fe(ClO_4)_3$. (d) Absorption spectra of PT3 (1×10^{-5} M) in CH_3Cl in the presence of different amounts of sodium ascorbate.

Benefiting from the electron-donating properties of TTF, it is expected that the most stable conformation for PT3/PT5 under Fe^{3+} oxidation is the conformation in which the TTF unit occupies the electron-rich cavity of the pillar[5]arene. As shown in Figure 2a, UV−vis absorption spectra show that the TTF unit can be oxidized by gradually adding $Fe(ClO_4)_3$. As reported in the literature, 1 equiv Fe^{3+} can quantitatively oxidize TTF derivatives into corresponding cation radicals. The TTF derivative can be further oxidized to the form of dications under the oxidation of Fe^{3+} exceeding 1 equiv.[47] For control molecule A (Figures S26 and S27, Supporting Information), due to the oxidation of Fe^{3+}, two new absorption peaks appeared at about 430 and 634 nm, respectively, and the absorption intensity is gradually enhanced with the gradual increase of Fe^{3+}. When more than 1 equiv Fe^{3+} is added, the absorption intensities at about 430 and 634 nm started to decrease, and a new dications absorption band appeared at about 500 nm (Figure S28, Supporting Information). In contrast, flipping the ring units of PT3 can place the TTF unit inside of the pillar[5]arene cavity. As shown in Figure 2, after Fe^{3+} oxidation, the TTF unit flips into the cavity of the pillar[5]arene to form a charge-transfer complex with an absorption at λ_{max} = 692 nm in CH_2Cl_2, indicating that the peak is red-shifted by 58 nm relative to molecule A. It is noteworthy that, in contrast to A, the TTF unit does not achieve a complete successive one-electron oxidation. With the addition of 1 equiv Fe^{3+}, the peak at 692 nm gradually intensified and stabilized. After further adding more than 1 equiv Fe^{3+}, the UV absorption intensity of $PT3^{\bullet+}$ radical cation decreases, similar to the formation of the $PT3^{2+}$ dication. This discontinuous oxidation may be mainly attributed to the protection of fulvalene radical cations by pillar[5]arenes, and the cavity effect of this macrocycle was more pronounced on PT5. As shown in Figures S29−S31, the charge-transfer absorption band of PT5 appeared at a significantly higher wavelength of λ_{max} = 709 nm. However, the absorption band at 709 nm was not weakened by stepwise addition of Fe^{3+} to 2 equiv, indicating that the TTF unit exists stably in the cavity of the pillar[5]arene in the form of radical cations ($PT5^{\bullet+}$). This change in the UV−vis spectroscopy can also be distinguished by the color change of the solution; that is, the pale-yellow solution of PT3 turned pale green after adding more than 1 equiv Fe^{3+}. Electrochemical experiments showed that without any oxidant, the color of the PT3 solution became lighter with no obvious tone change. The above color change is mainly due to the oxidation of Fe^{3+} that results in free Fe^{2+} (light green). The reversibility of the process is demonstrated by gradually adding the reducing agent, sodium ascorbate. In comparison with Figures 2b and S29, Figures 2d and S31 show reversed spectral changes, and the original spectrum is restored when 2 equiv sodium ascorbate was added. This phenomenon indicates that under redox triggering, PT3/PT5 can place the TTF unit inside or outside of the pillar[5]arene cavity.

The density functional theory (DFT) calculation by the Gaussian 16 program further deepens the understanding of molecular binding modes. After conformational search, the most stable isomers of PT3-out-pR, PT3-in-pS, PT5-out-pR, and PT5-in-pS are screened out and shown in Figure 3 (see Figure S32 and Table S1 for other isomers and their energies). The Gibbs free-energy changes for the oxidation processes of PT3-out-pR and PT5-out-pR are very negative values of −263.55 and −148.77 kcal/mol, respectively, which suggests that both species should be able to be oxidized by Fe^{3+}. This result is consistent with the experimental result.

https://doi.org/10.1021/jacs.3c04430
J. Am. Chem. Soc. 2023, 145, 16711−16717

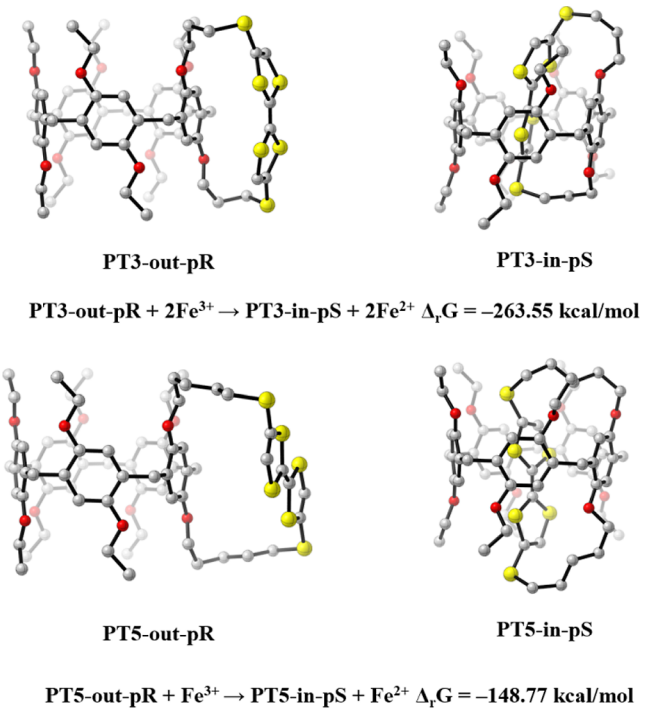

Figure 3. Optimized geometries of the most stable isomers of PT3-out-pR, PT3-in-pS, PT5-out-pR, and PT5-in-pS. For the sake of clarity, hydrogen atoms are not shown here. The Gibbs free-energy changes for the oxidation processes of PT3-out-pR and PT5-out-pR are listed here.

To investigate the oxidative processes of PT3 and PT5, cyclic voltammetry (CV) experiments were also performed. Figures S33 and S34 show the anodic behavior of PT3 and PT5. With 0.1 M tetrabutylammonium chloride (TBACl) as the supporting electrolyte, PT3 in dichloromethane solution shows reversible two-electron oxidation, with peak potentials of 0.58 and 0.85 V, while PT5 shows reversible one-electron redox, where the potential difference (ΔE_p) is ca. 0.07 V. Compared with the PT3 with a shorter flexible alkyl chain, the TTF unit on PT5 seems to be more accessible to the cavities of pillar[5]arene, and the one-electron redox exhibited by PT5 may be mainly attributed to the protection of fulvalene radical cations by pillar[5]arenes. By adding $Fe(ClO_4)_3$ to the MeCN solution of degassed PT3 and PT5, solutions in different oxidation states were prepared, and the radical species in the solution in the oxidation state were studied by electron paramagnetic resonance (EPR) spectroscopy. As shown in Figures S35 and S36, both systems PT3/1 equiv Fe^{3+} (g = 2.0102, a = 0) and PT3/2 equiv Fe^{3+} (g = 2.0101, a = 0) produced strong EPR signals. However, compared with the PT3/1 equiv Fe^{3+} system, the EPR signal of the PT3/2 equiv Fe^{3+} system was weakened, which confirms that the PT3 cationic radical transformed to the dication. In contrast, the EPR signals of the PT5/1 equiv Fe^{3+} (g = 2.0213, a = 0) and PT5/2 equiv Fe^{3+} (g = 2.0210, a = 0) systems did not change significantly.

To confirm that the fused tetrathiafulvalene led to a pair of isolable enantiomers, we performed chiral separation and circular dichroism (CD) spectroscopy experiments. After injecting the racemic mixture into a preparative chiral HPLC column, two peaks (F1 and F2) of equal area were observed (Figures 4a and S37, Supporting Information). As shown in

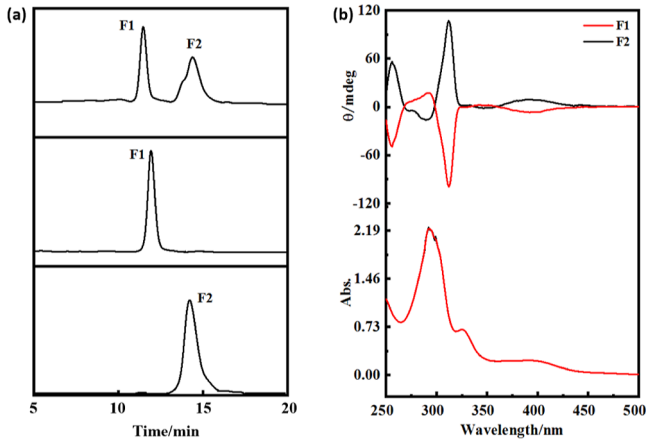

Figure 4. (a) HPLC traces of PT3, the first fraction (F1) of PT3, and the second fraction (F2) of PT3. (b) CD and UV−vis spectra (0.1 mM) of F1 and F2 in chloroform at 25 °C.

Figure 4a, the retention time of F1 and F2 on HPLC is the same as the two peaks of racemate, indicating a pair of pure isomers, which were measured by CD and UV−vis spectra (Figures 4b and S38, Supporting Information). In chloroform, the Cotton effect of F1 was negative at 309 nm, while F2 exhibited a positive effect with the CD signals at 390 nm. The CD spectrum of F1 is completely mirror symmetric to that of F2, indicating that they are a pair of enantiomers. The Sp (Sp, Sp, Sp, Sp, Sp) configuration of pillar[5]arenes has been reported to generate a negative CD extremum (CDex) at 310 nm; therefore, the absolute configuration of pillar[5]arenes can be assigned by CD spectroscopy. Here, F1 and F2 fractions are assigned as out-pS and out-pR, respectively. The turnover of the PT3/PT5 side ring can make the TTF unit roll into/out of the cavity of pillar[5]arenes, resulting in chiral inversion of the pillar[5]arenes core.

Considering that the binding of the pillar[5]arenes host to the TTF dication compared to the reduced from of TTF is stronger by several orders of magnitude, we think that it may be possible to control the chiral inversion of PT3/PT5 through redox. The CD spectrum shows that with the increase in oxidant $Fe(ClO_4)_3$ from 0.1 to 1 equiv, the CD spectral signal of PT3-F2 in dichloromethane solution decreased to a minimum at 1 equiv, and further addition of $Fe(ClO_4)_3$ resulted in CD signal inverts from positive to negative at 309 nm (Figure 5a), indicating that a chirality inversion from out-Sp to in-Rp occurred after oxidation. The CD signal reaches a negative maximum after adding 2 equiv $Fe(ClO_4)_3$. In addition, this inversion is completely reversible. As shown in Figure 5b, after adding 2 equiv of the reducing agent, sodium ascorbate, the inverted CD spectrum of PT3-F2 completely restored to the original state. For PT5, as the oxidant $Fe(ClO_4)_3$ increased from 0.1 to 1 equiv, the CD signal reversed from positive to negative, and chirality inversion was also achieved. Similarly, the inverted CD spectrum of PT5-F1 can be completely restored to the original state after adding 1 equiv of sodium ascorbate (Figures S39 and S40, Supporting Information). PT3 with a shorter aliphatic linker generates the corresponding radical cation under the oxidation of 0−1 equiv of $Fe(ClO_4)_3$, and the chirality gradually weakens at this time, indicating that the TTF unit has been inverted. Under the oxidation of 1−2 equiv of $Fe(ClO_4)_3$, the dication form is further generated, and the TTF unit further occupies the

https://doi.org/10.1021/jacs.3c04430
J. Am. Chem. Soc. 2023, 145, 16711−16717

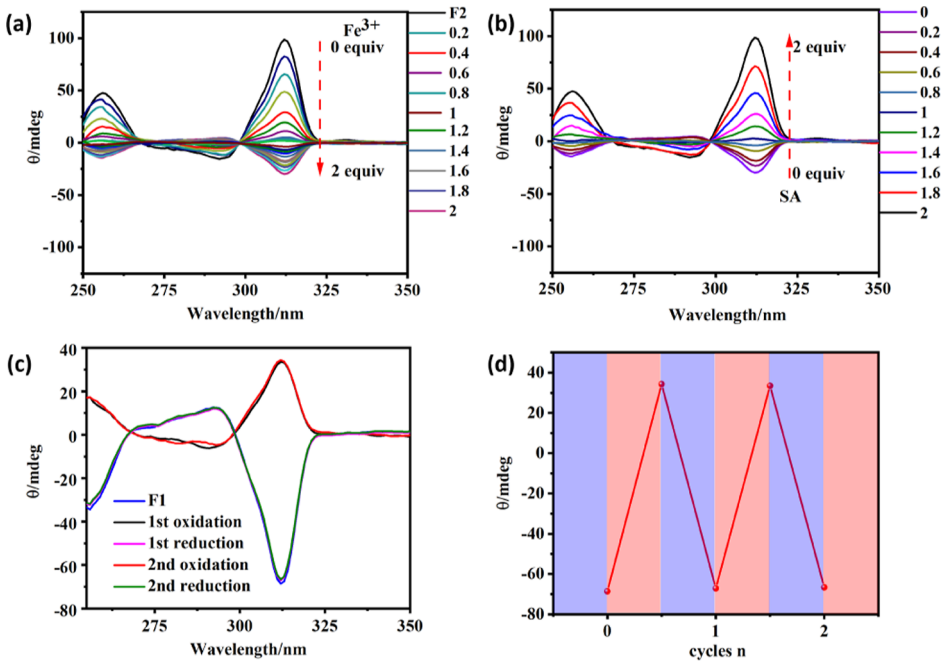

Figure 5. (a) CD spectrum of PT3-F2 in chloroform under $Fe(ClO_4)_3$ oxidation at 25 °C (0.1 mM). (b) CD spectrum of PT3-F2 in chloroform under sodium ascorbate reduction at 25 °C (0.1 mM). (c) Reversibility of the redox process of PT3-F1. (d) Relationship between the CD value of PT3-F1 at 310 nm and the number of cycles.

pillar[5]arene cavity due to the stronger binding, realizing the chiral stepping inversion. For PT5 with a longer aliphatic linker, due to the more flexible aliphatic linker, under the oxidation of 0−1 equiv $Fe(ClO_4)_3$, the TTF unit is flipped into the cavity of the pillar[5]arene to realize the chirality inversion; the TTF units are more likely to exist stably in the form of radical cations at this time, since there is no obvious change in the CD signal of PT5 when more than 1 equiv $Fe(ClO_4)_3$ is added. In order to further prove the reduced form of TTF unit outside the cavity and oxidized form of TTF in the cavity, the collision cross section (CCS) analysis was performed. First, the mass spectra of PT3 and PT5 before and after oxidation were obtained through Fourier transform ion cyclotron resonance (FT ICR) (Figure S41 and Supporting Information). Subsequently, the decay time constants of PT3 and PT5 before and after oxidation were calculated by eq S1.[48] By using the decay time constant, the cross section (Å^2) of PT3, PT3 + Fe^{3+}, PT5, and PT5 + Fe^{3+} were calculated according to eq S2,[48] and the results showed that $Å^2_{PT3} > Å^2_{PT3+Fe^{3+}}$ and $Å^2_{PT5} > Å^2_{PT5+Fe^{3+}}$ (Figure S42, Supporting Information). The CCS analysis demonstrated that the cross section of the oxidized form PT3/PT5 is smaller than that of the reduced form PT3/PT5, confirming that the oxidized form of the TTF unit was in the cavity of PT3/PT5 and the reduced form was outside the cavity of PT3/PT5. In addition, after adding more than 2 equiv Hg^{2+}, two-dimensional ROESY NMR spectra of PT3 and PT5 were obtained. As shown in Figures S43 and S44, the disappearance of the protons on the TTF fused rings indicates sufficient oxidation. Significant NOE signals were observed between the proton H_a of the alkyl chain and the protons H_b of the benzene ring as well as the protons H_c of methylene, indicating that the oxidized TTF unit entered the cavity of the pillar[5]arene, further leading to the chiral inversion of PT3 and PT5, while no such signals were observed for the unoxidized PT3 and PT5 (Figures S45 and S46, Supporting Information). On the other hand, cyclic oxidation and reduction of TTF units were achieved through electrochemical experiments, which led to reversible switching of the CD signal, and the signal intensity did not decrease significantly after two cycles (Figure 5c,d). Interestingly, whether PT3 or PT5 solution is used, the solution will change from light yellow to light green after chiral inversion. Furthermore, the CD spectral changes of PT3-F1 at different temperatures in different solvents were also investigated (Figures S47−S52, Supporting Information).

CONCLUSIONS

In summary, a new unimolecular chiral stepping inversion molecular machine (SIMM) was constructed by fusing a redox-active TTF onto one repeating unit of a pillar[5]arene through alkyl chains of different lengths. Benefiting from the electron-donating properties of tetrathiafulvalene, redox-triggered chiral inversion was achieved. Interestingly, PT3 with a shorter aliphatic linker exhibited a tendency for stepping inversion, achieving chiral inversion under two-electron redox, while PT5 with a longer aliphatic linker achieved one-electron redox chirality inversion. In addition, the change in molecular chirality was accompanied by a change in solution color, so the molecular chirality can be identified by the solution color.

ASSOCIATED CONTENT

Supporting Information

The Supporting Information is available free of charge at https://pubs.acs.org/doi/10.1021/jacs.3c04430

Compound characterization, Job plot, K_a value, CD spectra, CV experiments, EPR spectroscopy, UV−vis spectra, chiral HPLC trace, 2D NOESY NMR spectra, 2D ROESY NMR spectra, and collision cross section analysis (PDF)

https://doi.org/10.1021/jacs.3c04430
J. Am. Chem. Soc. 2023, 145, 16711−16717

AUTHOR INFORMATION

Corresponding Author

Yu Liu − *College of Chemistry, State Key Laboratory of Elemento-Organic Chemistry, Nankai University, Tianjin 300071, P. R. China;* orcid.org/0000-0001-8723-1896; Email: yuliu@nankai.edu.cn

Authors

Yonghui Sun − *College of Chemistry, State Key Laboratory of Elemento-Organic Chemistry, Nankai University, Tianjin 300071, P. R. China*

Lijuan Liu − *College of Chemistry, State Key Laboratory of Elemento-Organic Chemistry, Nankai University, Tianjin 300071, P. R. China*

Linnan Jiang − *College of Chemistry, State Key Laboratory of Elemento-Organic Chemistry, Nankai University, Tianjin 300071, P. R. China*

Yong Chen − *College of Chemistry, State Key Laboratory of Elemento-Organic Chemistry, Nankai University, Tianjin 300071, P. R. China*

Hengyue Zhang − *College of Chemistry, State Key Laboratory of Elemento-Organic Chemistry, Nankai University, Tianjin 300071, P. R. China*

Xiufang Xu − *College of Chemistry, State Key Laboratory of Elemento-Organic Chemistry, Nankai University, Tianjin 300071, P. R. China;* orcid.org/0000-0002-3510-3267

Complete contact information is available at: https://pubs.acs.org/10.1021/jacs.3c04430

Notes

The authors declare no competing financial interest.

ACKNOWLEDGMENTS

This work was financially supported by the National Natural Science Foundation of China (grants 22131008, 21971127 and 21873051) and the Fundamental Research Funds for the Central Universities, Nankai University.

REFERENCES

(1) van Dijk, L.; Tilby, M. J.; Szpera, R.; Smith, O. A.; Bunce, H. A. P.; Fletcher, S. P. Molecular machines for catalysis. *Nat. Rev. Chem.* **2018**, *2*, 0117.

(2) Watson, M. A.; Cockroft, S. L. Man-made molecular machines: membrane bound. *Chem. Soc. Rev.* **2016**, *45*, 6118−6129.

(3) Garcia-Lopez, V.; Chen, F.; Nilewski, L. G.; Duret, G.; Aliyan, A.; Kolomeisky, A. B.; Robinson, J. T.; Wang, G. F.; Pal, R.; Tour, J. M. Molecular machines open cell membranes. *Nature* **2017**, *548*, 567−572.

(4) Aprahamian, I. The Future of Molecular Machines. *ACS Cent. Sci.* **2020**, *6*, 347−358.

(5) Ortega, D. R.; Yang, W.; Subramanian, P.; Mann, P.; Kjaer, A.; Chen, S. Y.; Watts, K. J.; Pirbadian, S.; Collins, D. A.; Kooger, R.; Kalyuzhnaya, M. G.; Ringgaard, S.; Briegel, A.; Jensen, G. J. Repurposing a chemosensory macromolecular machine. *Nat. Commun.* **2020**, *11*, 2041.

(6) Yang, L. P.; Wang, X. P.; Yao, H.; Jiang, W. Naphthotubes: Macrocyclic Hosts with a Biomimetic Cavity Feature. *Acc. Chem. Res.* **2020**, *53*, 198−208.

(7) Dong, J. Q.; Li, X.; Zhang, K.; Di Yuan, Y.; Wang, Y. X.; Zhai, L. Z.; Liu, G. L.; Yuan, D. Q.; Jiang, J. W.; Zhao, D. Confinement of Aggregation-Induced Emission Molecular Rotors in Ultrathin Two-Dimensional Porous Organic Nanosheets for Enhanced Molecular Recognition. *J. Am. Chem. Soc.* **2018**, *140*, 4035−4046.

(8) Mukhopadhyay, R. D.; Das, G.; Ajayaghosh, A. Stepwise control of host−guest interaction using a coordination polymer gel. *Nat. Commun.* **2018**, *9*, 1987.

(9) Heard, A. W.; Goldup, S. M. Synthesis of a Mechanically Planar Chiral Rotaxane Ligand for Enantioselective Catalysis. *Chem* **2020**, *6*, 994−1006.

(10) Powers, I. G.; Andjaba, J. M.; Luo, X. Y.; Mei, J. G.; Uyeda, C. Catalytic Azoarene Synthesis from Aryl Azides Enabled by a Dinuclear Ni Complex. *J. Am. Chem. Soc.* **2018**, *140*, 4110−4118.

(11) Corra, S.; Curcio, M.; Baroncini, M.; Silvi, S.; Credi, A. Photoactivated Artificial Molecular Machines that Can Perform Tasks. *Adv. Mater.* **2020**, *32*, 1906064.

(12) Si, W.; Yu, M.; Wu, G. S.; Chen, C.; Sha, J. J.; Zhang, Y.; Chen, Y. F. A Nanoparticle-DNA Assembled Nanorobot Powered by Charge-Tunable Quad-Nanopore System. *ACS Nano* **2020**, *14*, 15349−15360.

(13) Li, Z.; Song, N.; Yang, Y. W. Stimuli-Responsive Drug-Delivery Systems Based on Supramolecular Nanovalves. *Matter* **2019**, *1*, 345−368.

(14) Amodio, A.; Del Grosso, E.; Troina, A.; Placidi, E.; Ricci, F. Remote Electronic Control of DNA-Based Reactions and Nanostructure Assembly. *Nano Lett.* **2018**, *18*, 2918−2923.

(15) Shimomura, K.; Ikai, T.; Kanoh, S.; Yashima, E.; Maeda, K. Switchable enantioseparation based on macromolecular memory of a helical polyacetylene in the solid state. *Nat. Chem.* **2014**, *6*, 429−434.

(16) Salikolimi, K.; Praveen, V. K.; Sudhakar, A. A.; Yamada, K.; Horimoto, N. N.; Ishida, Y. Helical supramolecular polymers with rationally designed binding sites for chiral guest recognition. *Nat. Commun.* **2020**, *11*, 2311.

(17) Wang, C. X.; Wang, S. K.; Yang, H. T.; Xiang, Y. X.; Wang, X. B.; Bao, C. Y.; Zhu, L. Y.; Tian, H.; Qu, D. H. A Light-Operated Molecular Cable Car for Gated Ion Transport. *Angew. Chem., Int. Ed.* **2021**, *60*, 14836−14840.

(18) Wankar, J.; Kotla, N. G.; Gera, S.; Rasala, S.; Pandit, A.; Rochev, Y. A. Recent Advances in Host-Guest Self-Assembled Cyclodextrin Carriers: Implications for Responsive Drug Delivery and Biomedical Engineering. *Adv. Funct. Mater.* **2020**, *30*, 1909049.

(19) Kumar, R.; Sharma, A.; Singh, H.; Suating, P.; Kim, H. S.; Sunwoo, K.; Shim, I.; Gibb, B. C.; Kim, J. S. Revisiting Fluorescent Calixarenes: From Molecular Sensors to Smart Materials. *Chem. Rev.* **2019**, *119*, 9657−9721.

(20) Li, S. H.; Zhang, H. Y.; Xu, X. F.; Liu, Y. Mechanically selflocked chiral gemini-catenanes. *Nat. Commun.* **2015**, *6*, 7590.

(21) Chen, J. F.; Yin, X. D.; Wang, B. W.; Zhang, K.; Meng, G. Y.; Zhang, S. H.; Shi, Y. F.; Wang, N.; Wang, S. N.; Chen, P. K. Planar Chiral Organoboranes with Thermoresponsive Emission and Circularly Polarized Luminescence: Integration of Pillar[5]arenes with Boron Chemistry. *Angew. Chem., Int. Ed.* **2020**, *59*, 11267−11272.

(22) Fa, S. X.; Egami, K.; Adachi, K.; Kato, K.; Ogoshi, T. Sequential Chiral Induction and Regulator-Assisted Chiral Memory of Pillar[5]-arenes. *Angew. Chem., Int. Ed.* **2020**, *59*, 20353−20356.

(23) Zhu, H. T. Z.; Li, Q.; Shi, B. B.; Xing, H.; Sun, Y.; Lu, S.; Shangguan, L. Q.; Li, X. P.; Huang, F. H.; Stang, P. J. Formation of Planar Chiral Platinum Triangles via Pillar[5]arene for Circularly Polarized Luminescence. *J. Am. Chem. Soc.* **2020**, *142*, 17340−17345.

(24) Ji, J. C.; Wei, X. Q.; Wu, W. H.; Fan, C. Y.; Zhou, D. Y.; Kanagaraj, K.; Cheng, G.; Luo, K.; Meng, X. G.; Yang, C. The More the Slower: Self-Inhibition in Supramolecular Chirality Induction, Memory, Erasure, and Reversion. *J. Am. Chem. Soc.* **2022**, *144*, 1455−1463.

(25) Ogoshi, T.; Yamagishi, T. A.; Nakamoto, Y. Pillar-Shaped Macrocyclic Hosts Pillar n arenes: New Key Players for Supramolecular Chemistry. *Chem. Rev.* **2016**, *116*, 7937−8002.

(26) Murray, J.; Kim, K.; Ogoshi, T.; Yao, W.; Gibb, B. C. The aqueous supramolecular chemistry of cucurbit[n]urils, pillar[n]arenes and deep-cavity cavitands. *Chem. Soc. Rev.* **2017**, *46*, 2479−2496.

(27) Kakuta, T.; Yamagishi, T.; Ogoshi, T. Stimuli-Responsive Supramolecular Assemblies Constructed from Pillar[n]arenes. *Acc. Chem. Res.* **2018**, *51*, 1656−1666.
(28) Ogoshi, T.; Akutsu, T.; Yamafuji, D.; Aoki, T.; Yamagishi, T. Solvent- and Achiral-Guest-Triggered Chiral Inversion in a Planar Chiral *pseudo*[1]Catenane. *Angew. Chem., Int. Ed.* **2013**, *52*, 8111−8115.
(29) Yao, J. B.; Wu, W. H.; Liang, W. T.; Feng, Y. J.; Zhou, D. Y.; Chruma, J. J.; Fukuhara, G.; Mori, T.; Inoue, Y.; Yang, C. Temperature-Driven Planar Chirality Switching of a Pillar[5]arene-Based Molecular Universal Joint. *Angew. Chem., Int. Ed.* **2017**, *56*, 6869−6873.
(30) Liang, H. Z.; Hua, B.; Xu, F.; Gan, L. S.; Shao, L.; Huang, F. H. Acid/Base-Tunable Unimolecular Chirality Switching of a Pillar[5] azacrown Pseudo 1 Catenane. *J. Am. Chem. Soc.* **2020**, *142*, 19772−19778.
(31) Lee, E.; Ju, H.; Park, I. H.; Jung, J. H.; Ikeda, M.; Kuwahara, S.; Habata, Y.; Lee, S. S. Pseudo[1]Catenane-Type Pillar[5]thiacrown Whose Planar Chiral Inversion is Triggered by Metal Cation and Controlled by Anion. *J. Am. Chem. Soc.* **2018**, *140*, 9669−9677.
(32) Yao, J. B.; Wu, W. H.; Xiao, C.; Su, D.; Zhong, Z. H.; Mori, T.; Yang, C. Overtemperature-protection intelligent molecular chiroptical photoswitches. *Nat. Commun.* **2021**, *12*, 2600.
(33) Zhou, Q.; Song, K.; Zhang, G. X.; Song, X. W.; Lin, J. F.; Zang, Y. P.; Zhang, D. Q.; Zhu, D. B. Tetrathiafulvalenes as anchors for building highly conductive and mechanically tunable molecular junctions. *Nat. Commun.* **2022**, *13*, 1803.
(34) Goeb, S.; Salle, M. Electron-rich Coordination Receptors Based on Tetrathiafulvalene Derivatives: Controlling the Host-Guest Binding. *Acc. Chem. Res.* **2021**, *54*, 1043−1055.
(35) Jana, A.; Bahring, S.; Ishida, M.; Goeb, S.; Canevet, D.; Salle, M.; Jeppesen, J. O.; Sessler, J. L. Functionalised tetrathiafulvalene-(TTF-) macrocycles: recent trends in applied supramolecular chemistry. *Chem. Soc. Rev.* **2018**, *47*, 5614−5645.
(36) Park, J. S.; Sessler, J. L. Tetrathiafulvalene (TTF)-Annulated Calix[4]pyrroles: Chemically Switchable Systems with Encodable Allosteric Recognition and Logic Gate Functions. *Acc. Chem. Res.* **2018**, *51*, 2400−2410.
(37) Wu, Y. L.; Frasconi, M.; Liu, W. G.; Young, R. M.; Goddard, W. A.; Wasielewski, M. R.; Stoddart, J. F. Electrochemical Switching of a Fluorescent Molecular Rotor Embedded within a Bistable Rotaxane. *J. Am. Chem. Soc.* **2020**, *142*, 11835−11846.
(38) Wu, Q.; Xie, R. K.; Mao, M. J.; Chai, G. L.; Yi, J. D.; Zhao, S. S.; Huang, Y. B.; Cao, R. Integration of Strong Electron Transporter Tetrathiafulvalene into Metalloporphyrin-Based Covalent Organic Framework for Highly Efficient Electroreduction of CO2. *ACS Energy Lett.* **2020**, *5*, 1005−1012.
(39) Verma, P.; Singh, A.; Rahimi, F. A.; Sarkar, P.; Nath, S.; Pati, S. K.; Maji, T. K. Charge-transfer regulated visible light driven photocatalytic H-2 production and CO2 reduction in tetrathiafulvalene based coordination polymer gel. *Nat. Commun.* **2021**, *12*, 7313.
(40) Schroder, H. V.; Stein, F.; Wollschlager, J. M.; Sobottka, S.; Gaedke, M.; Sarkar, B.; Schalley, C. A. Accordion-Like Motion in Electrochemically Switchable Crown Ether/Ammonium Oligorotaxanes. *Angew. Chem., Int. Ed.* **2019**, *58*, 3496−3500.
(41) Jia, F.; Schroder, H. V.; Yang, L. P.; von Essen, C.; Sobottka, S.; Sarkar, B.; Rissanen, K.; Jiang, W.; Schalley, C. A. Redox-Responsive Host-Guest Chemistry of a Flexible Cage with Naphthalene Walls. *J. Am. Chem. Soc.* **2020**, *142*, 3306−3310.
(42) Vicent-Morales, M.; Esteve-Rochina, M.; Calbo, J.; Orti, E.; Vitorica-Yrezabal, I. J.; Mínguez Espallargas, G. Semiconductor Porous Hydrogen-Bonded Organic Frameworks Based on Tetrathiafulvalene Derivatives. *J. Am. Chem. Soc.* **2022**, *144*, 9074−9082.
(43) Zhou, Y.; Hu, Q.; Yu, F.; Ran, G. Y.; Wang, H. Y.; Shepherd, N. D.; D'Alessandro, D. M.; Kurmoo, M.; Zuo, J. L. A Metal-Organic Framework Based on a Nickel Bis(dithiolene) Connector: Synthesis, Crystal Structure, and Application as an Electrochemical Glucose Sensor. *J. Am. Chem. Soc.* **2020**, *142*, 20313−20317.
(44) Zhao, Y. L.; Dichtel, W. R.; Trabolsi, A.; Saha, S.; Aprahamian, I.; Stoddart, J. F. A Redox-Switchable α-Cyclodextrin-Based [2]-Rotaxane. *J. Am. Chem. Soc.* **2008**, *130*, 11294−11296.
(45) Ogoshi, T.; Kanai, S.; Fujinami, S.; Yamagishi, T. A.; Nakamoto, Y. *para*-bridged symmetrical Pillar[5]arenes: Their Lewis Acid Catalyzed Synthesis and Host-Guest property. *J. Am. Chem. Soc.* **2008**, *130*, 5022−5023.
(46) Li, C. J.; Xu, Q. Q.; Li, J.; Yao, F. N.; Jia, X. S. Complex interactions of pillar[5]arene with paraquats and bis(pyridinium) derivatives. *Org. Biomol. Chem.* **2010**, *8*, 1568−1576.
(47) Sun, J. L.; Wu, Y. L.; Wang, Y. P.; Liu, Z. C.; Cheng, C. Y.; Hartlieb, K. J.; Wasielewski, M. R.; Stoddart, J. F. An Electrochromic Tristable Molecular Switch. *J. Am. Chem. Soc.* **2015**, *137*, 13484−13487.
(48) Zhou, M.; Jiao, L.; Xu, S.; Xu, Y.; Du, M.; Zhang, X.; Kong, X. A novel method for photon unfolding spectroscopy of protein ions in the gas phase. *Rev. Sci. Instrum.* **2022**, *93*, 043003.

https://doi.org/10.1021/jacs.3c04430
J. Am. Chem. Soc. 2023, 145, 16711−16717